Contact Mechanics of UV/Ozone-Treated PDMS by AFM and JKR Testing: Mechanical Performance from Nano- to Micrometer Length Scales

Jing Song, Davide Tranchida, and G. Julius Vancso*

Dutch Polymer Institute and MESA+ Institute for Nanotechnology, Materials Science and Technology of Polymers, University of Twente, P.O. Box 217, 7500 AE Enschede, The Netherlands

Received March 10, 2008; Revised Manuscript Received July 7, 2008

ABSTRACT: The Young's modulus of cross-linked poly(dimethylsiloxane) (PDMS) surface was quantitatively investigated as a function of UV/ozone treatment time across different length scales. An AFM was used to probe PDMS surface mechanical properties at the nanometer length scale. The Young's modulus of each sample was estimated with continuum contact mechanics theory (Sneddon method) using AFM data by employing the hyperboloid tip shape model. A custom-built ATD device (JKR method) was also used which allowed us to simultaneously monitor the load, the contact area, and the relative displacement between (a) a lens (made either of PDMS elastomer or of Si_3N_4) and (b) surface-treated PDMS films upon loading and unloading on the micrometer to submillimeter length scales. The modulus of PDMS increased with increasing treatment time as observed by AFM as well as by ATD, which we explained by the gradual formation of a silica-like layer. For all specimens tested, the modulus values obtained were highest from AFM, lower from ATD, and lowest from bulk tensile experiments for the same UV/ozone dose. These results demonstrate the effect of the probed length scale of the tests used to assess mechanical performance.

Introduction

Mechanical properties of surfaces and interfaces are important for the understanding of the behavior of adhesive and sliding contacts.[1] In addition, mechanical response of elastomers is one of other important concerns in some applications such as tunable microdoublet lenses[2] and dielectric elastomer actuators.[3] A widely used elastomer, cross-linked PDMS, has been applied in several areas such as thin films and coatings, soft lithography, biomedical applications, optical systems, nanotribology, nanofluidics, MEMS/NEMS, etc.[4,5] These applications require an understanding and precise, quantitative characterization of the mechanical properties of PDMS from the nanometer to the macroscopic length scales.

As well-known, surface treatment can result in changes of surface properties. In our previous studies,[6,7] the changes of surface chemistry and ionization state of PDMS exposed to UV/ozone irradiation have been reported. It has been shown that, during treatment-dependent surface modifications of PDMS, silanol groups were introduced at the surface. Oxidative cross-linking via Si−O bridges was found to cause the gradual formation of a continuous "silica-like" barrier layer, supported also by X-ray photoelectron spectroscopy (XPS).[8] This thin silica-like layer should affect the mechanical properties of the treated PDMS surface. In addition, as the characteristic dimensions of the mechanical tests are reduced, the observed effective surface properties may greatly vary. Despite the widespread use of untreated and surface-treated PDMS, the characteristic length scale effects on mechanical properties have not been quantitatively studied. Hence, in this work we address the variation in modulus related to the indentation size, indentation depth, and treatment dose. Our studies also demonstrate the effect of the probed length scale on the value of the observed mechanical properties.

Recently, indentation techniques have been extensively used for mechanical characterization of materials. Development of instrumented indentation techniques at low and ultralow load levels has improved their utility for understanding the mechanical responses of solids at micro- and nanometer length scales. In this paper, two indentation instruments, i.e., atomic force microscopy (AFM) and adhesion testing device (ATD), were chosen to investigate the influence of surface treatment upon the elastic modulus of PDMS obtained from nano- and microindentations. Advances of AFM enable the quantitative examination of surface mechanical properties with substantially improved force and spatial resolution. Here, an analysis method, partly derived from the Sneddon model, and taking into account adhesion by using a hyperboloid tip, was applied. Subsequently, the ATD technique provided a direct evaluation of elastic modulus at the micrometer length scale. Finally, a comparison of PDMS's response against nano- and microdeformation to its bulk properties was reported. We anticipate that this study of PDMS near-to-surface mechanical properties would be valuable for material selection and design improvements in a number of practical applications.

Surface Young's Modulus at the Nanoscopic Length Scale

There are two different methods commonly used for the measurement of indentation which are called the "imaging method" and "compliance method".[9] In the imaging method, the indentor penetrates in the sample surface with a specific load and retracts after a specific dwelling or residence time. The diameter or diagonal of the residual image of the indentation trace is then measured by optical or other methods. However, this method has some inherent limitations. The imaging of the residual indent becomes inexact as the indentation size is scaled down, and moreover, considerable viscoelastic recovery with time of the residual imprint can take place.[10] Therefore, this method provides primarily the plastic response of the material, or the viscoelastic−plastic properties of organic polymers, which creep in the indentation region significantly after unloading. Although Flores et al. provided a method to link the microhardness imprint to Young's modulus,[11] the so-called "imaging method" is not very suitable for obtaining information on the elastic behavior of the sample. This difficulty has been largely

* Corresponding author. E-mail: g.j.vancso@utwente.nl.

10.1021/ma800536y CCC: $40.75
Published on Web 08/22/2008

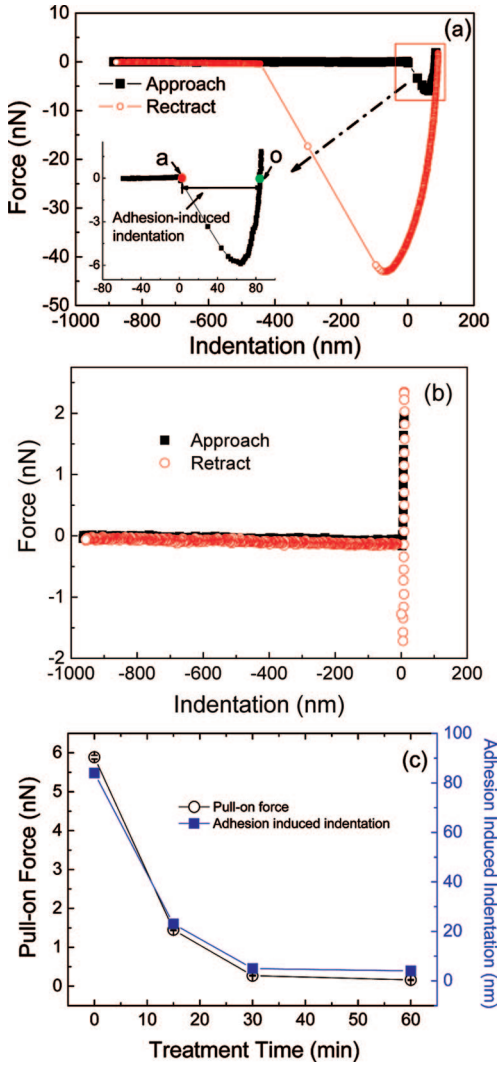

Figure 1. (a) Representative force indentation curve of pure, untreated PDMS. (b) Force indentation curve of 60 min treated PDMS. The Z scan size was set to 1 μm, and the Z scan rate was 1 Hz. (c) Pull-on force between the AFM tip and the PDMS surface, and adhesion-induced indentation as a function of UV/ozone treatment time. A commercial Si_3N_4 tip was used. To minimize the capillary force effect, all measurements were obtained under water. The value of the relative trigger was set to 20 nm.

overcome with the broad introduction of the "compliance method". The surface mechanical properties such as stiffness, hardness, and elastic modulus are obtained from the analysis of the load−displacement data recorded during loading−unloading indentation cycles performed upon material surfaces.

Using the AFM as a depth sensing instrument (DSI), the compliance method can be exploited in order to eliminate the need to visualize the indents. This technique has been used to study properties of polymeric materials with small dimensions (e.g., thin films and nano/microstructures) employing low indentation loads.[12,13] Several recent publications have demonstrated that reproducible and quantitative results could be obtained for a variety of polymers.[14−23] Various nanomechanical properties of polymer thin films, including elasticity,[24,25] hardness,[26] and viscoelasticity,[10,27−29] were studied.

A typical force vs indentation plot of untreated PDMS is given in Figure 1a. As can be seen, when the gradient of the interaction force exceeds the spring constant of the cantilever, k_c, the tip will jump in contact with the surface. The maximum value of the attractive force is defined as the pull-on force. Once the tip contacts the surface, the tip penetrates into the sample due to

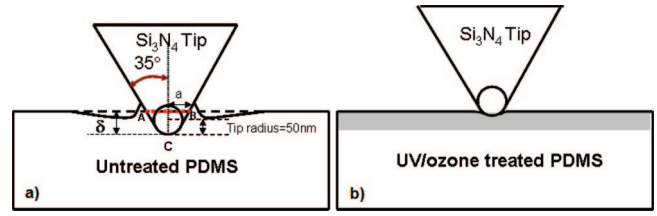

Figure 2. Schematic representation (not to scale) of a tip indenting due to the adhesive interaction: (a) untreated PDMS; (b) UV/ozone-treated PDMS.

the adhesive force between the tip and PDMS film.[30] When the AFM tip is retracted from a soft sample, the sample surface can be deformed by the pulling due to adhesive interactions. The pull-off force, i.e., the product of maximum contact cantilever deflection and k_c, is equal to the adherence, F_{ad}.

As shown earlier,[31] we considered that the surface of 60 min UV/ozone-treated PDMS films was fully oxidized. A typical force indentation curve for such a sample is shown in Figure 1b. Compared to untreated PDMS, the value of the pull-on force decreased from 5.9 to 0.2 nN and the pull-off force decreased from 43.1 to 1.7 nN. As the load applied on the tip was in the range between 0.1 and 2.0 nN during nanoindentations, adhesive forces must be taken into account because their contributions are significant as compared to purely elastic forces (see later).

The determination of the zero contact point in AFM indentation experiments using adhesive contact models is not without controversy. In this paper, we consider the initial contact as the point where the interaction becomes attractive, as defined by Walker and coauthors (shown in Figure 1a, as point "a").[30] At point "o" (see Figure 1a), where the AFM tip is pulled into the sample surface by adhesive interactions, the stored elastic energy and the surface energy are balanced; hence, there is a zero external force on the AFM cantilever. The indentation between the initial contact point "a" and point "o" is defined as the adhesion-induced indentation. Figure 1c shows that the pull-on force and adhesion-induced indentation of treated PDMS films decreased with increasing treatment time.

The details of surface roughness characterization of similar films can be found in a previous study.[31] For untreated and oxidized PDMS films, the average surface roughness (R_a) obtained by AFM topography analysis (scan area is 5 × 5 μm) is in the range of 1−2 nm. In addition, the mean roughness values were not influenced by the UV/ozone exposure. The use of smooth sample surfaces can simplify the collection of force curves because topographical artifacts are minimized. Therefore, the sample can be modeled as a half-space, and a suitable geometry should be assumed for the AFM tip.

The elastic modulus was deduced directly from the force indentation curves. The Johnson−Kendall−Roberts (JKR) theory is commonly used in adhesive contact mechanics, e.g., to describe contact forces and indentation for a sphere (lens) and a flat surface.[32] Normally, the shape of the AFM tip is considered spherical. The JKR theory for the elastic contact is valid only for contact radius values, which are much smaller than the tip radius ($R \approx 50$ nm). This does not hold for soft, untreated PDMS films, which can have larger contact radius values even under a zero load. For instance, when the external force is zero, the adhesion-induced indentation of an AFM tip into an untreated PDMS sample is about 83 nm, which is larger than the 50 nm tip radius (see Figure 2a). For UV/ozone-treated PDMS, especially for full oxidized PDMS, adhesion-induced indentation of the tip is small (see Figure 2b).

When characterizing very soft samples, a realistic AFM tip shape must be considered, taking into account not only the conical shape of the AFM tip far from the apex but also the roundness at the tip apex itself. For example, a paraboloid

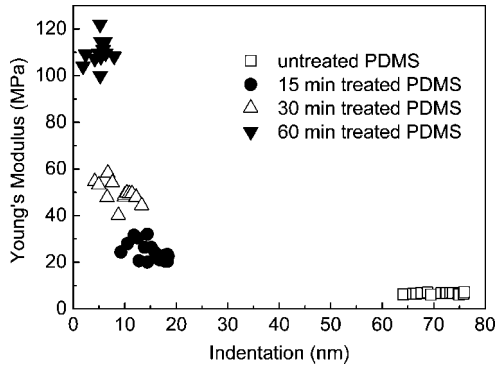

Figure 3. Young's modulus calculated with the hyperboloid shape tip model vs indentation depth: (□) pure PDMS; (○) 15 min treated PDMS; (△) 30 min treated PDMS; (▽) 60 min treated PDMS.

approximation for the tip shape has been successfully used until penetration depths of ~120 nm. In this work, because of the relatively large radius of standard Si_3N_4 tips, the shape was modeled by a hyperboloid.[30] The profile function for a hyperboloid shape tip is given by

$$f(x) = R\cot^2\alpha(((ax/R\cot\alpha)^2+1)^{1/2}-1) \quad (1)$$

where R is the radius of curvature of the tip apex, a is the contact radius, α is the tip semivertical angle as shown in Figure 2a, and x is the vertical distance to the tip apex (at point C, $x = 0$). To solve the dependence of the load and indentation on the contact radius, Walker et al.[30] used the original Sneddon's equations[33] relating applied load and penetration depth to contact radius for an indenter of arbitrary profile. In the case of an indenter with hyperboloid geometry and assuming that the rupture of the adhesive contact takes place according to Griffith's fracture theory,[34] the following equations were obtained:[30]

$$\delta = \frac{aA}{2R}\left[\frac{\pi}{2}+\arcsin\left(\frac{(a/A)^2-1}{(a/A)^2+1}\right)\right]-\left(\frac{2a\pi(1-v^2)W_{12}}{E}\right)^{1/2} \quad (2)$$

$$P = \frac{2E}{1-v^2}\left[\frac{A}{2R}\left[aA+\frac{a^2-A^2}{2}\left(\frac{\pi}{2}+\arcsin\frac{(a/A)^2-1}{(a/A)^2+1}\right)\right]-a\left(\frac{2a\pi(1-v^2)W_{12}}{E}\right)^{1/2}\right] \quad (3)$$

where $A = R\cot(\alpha)$, v is the Poisson ratio of PDMS, E is the elastic modulus of PDMS, and W_{12} is the interfacial energy of the tip and the sample. The sample elasticity can be obtained based on eqs 2 and 3 by combining point "o" (see Figure 1b) and any other point at the contact portion of the approaching curves "t". The detailed calculation is shown in the Supporting Information.

Figure 3 displays the values of the elastic moduli calculated by this method. It shows that the value of the modulus increases with increasing treatment time. In addition, for each sample, the Young's moduli do not show any significant variation with the indentation depth. The work of adhesion of each samples is, as expected,[35] in the order of 100 mJ/m^2. Therefore, adhesive forces between AFM tip and PDMS sample could not be neglected. Another issue, related to surface heterogeneity, should be noted as Hillborg and coauthors mentioned earlier.[8,31] Indeed, the stress field extends considerably over the hard silica layer permeating also into the soft rubbery sample beneath, and therefore the obtained values do not reflect the true modulus of the silica-like layer but should rather be considered as the sum of a laminate structure, with a high modulus surface layer on top of the PDMS elastomer. The presented data indicate the formation of a surface structure, which differs significantly from

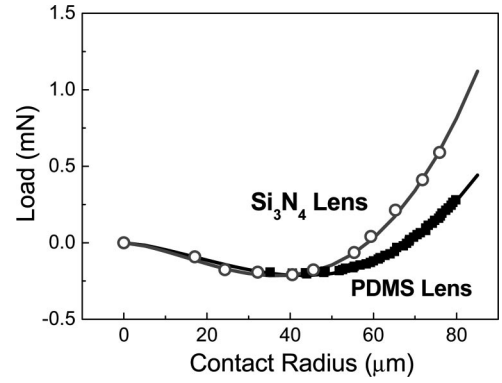

Figure 4. JKR fit to the advancing part of the loading of an untreated PDMS sample.

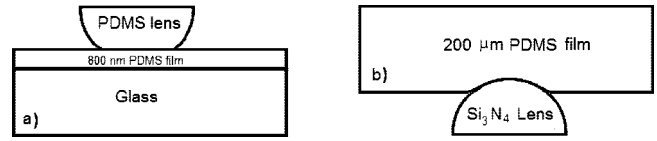

Figure 5. Schematic plot (not to scale) of lens and substrate combination: (a) PDMS lens; (b) Si_3N_4 lens.

that of silica which has an elastic modulus in the order of 70 GPa.[36]

Surface Young's Modulus at the Mesoscopic Length Scale

In order to assess the surface mechanical behavior of surface-treated PDMS films at the micrometer length scale, a custom-built, adhesion testing device (or a JKR-type contact mechanical apparatus) was used in this study.[35,37] This setup was used to describe the mechanics of contact that developed when a solid, hemispherical lens was pressed onto a flat substrate. The maximum contact radius was limited to 100 μm in order to keep the deformation in the elastic regime. Thus, the JKR model was applicable in this case. The relationship between the force and the contact radius of the loading and unloading part for contact between a PDMS or Si_3N_4 lens and a PDMS film is illustrated in Figure 4. The values of an "effective" thermodynamic work of adhesion (W) and combined elastic modulus (K) were obtained by fitting the recorded loading part using the JKR theory with eq 4. (We note that the JKR theory and eq 4 include thermodynamic work of adhesion. However, in practice, due to energy dissipative processes, work of adherence, or an "effective" work of adhesion, is measured.[37])

$$a^3 = \frac{R}{K}[P+3\pi RW_{12}+(6\pi RPW_{12}+(3\pi RW_{12})^2)^{1/2}] \quad (4)$$

In the ATD experiment, R is the relative radius, $1/R = 1/R_1 + 1/R_2$ (for an ideally flat surface, $R_2 \to \infty$), K is the combined elastic modulus $K = {}^4/_3[(1-v_1^2)/E_1 + (1-v_2^2)/E_2]^{-1}$ (with $E_{1,2}$ and $v_{1,2}$ as the elastic moduli and Poisson's ratios of the lens and sample film, respectively). In Figure 4, the filled data points correspond to the load vs contact radius relationship obtained with a PDMS lens on an untreated PDMS surface, fitted by eq 4 with W and K as fit parameters. The open circles in Figure 4 were obtained with a Si_3N_4 lens. The JKR fits are also shown.

Conventionally, ATD is used to study surface and interfacial properties between an elastomeric lens and a rigid substrate. The schematic plot of the arrangement of lens and film during the experiments is shown in Figure 5a. Compared to a hard substrate, a rubbery lens is easy to deform in the range of few micrometers. In our experiments, a new stiff Si_3N_4 indentor lens

Table 1. Young's Modulus Obtained with the ATD Method

	UV/ozone surface treatment time			
Young's modulus (MPa)	0 min	15 min	30 min	60 min
with a PDMS lens	3.9 ± 0.6	13.3 ± 2.8	24.4 ± 3.3	36.6 ± 4.8
with a Si_3N_4 lens	3.1 ± 0.5	8.6 ± 0.8	9.0 ± 1.2	13.1 ± 2.6

was also employed against relatively thick (200 μm) PDMS films in order to probe PDMS−Si_3N_4 interfaces, which are comparable to an AFM experiment regarding the chemical composition of the contacting surfaces (i.e., comparable interfacial energies). The corresponding experimental scheme is shown in Figure 5b. There are two advantages of using an Si_3N_4 indentor. (1) This geometry resembles a "scaled up" AFM tip−sample assembly: an enlarged AFM tip, i.e., the Si_3N_4 lens, and similar tip−sample contact geometry. Thus, length scale effects on surface modulus and adhesive forces over a larger length scale could be accessed. (2) Combined moduli obtained from JKR fitting procedures could be considered being approximately equal to the value of PDMS surface modulus without introducing a large error due to the high modulus of silicon nitride (220 GPa). However, there are still some disadvantages of using Si_3N_4 lenses. The surface roughness of Si_3N_4 lens is rather high ($R_a = 3.4 \pm 0.5$ nm) compared to normal PDMS lenses ($R_a = 1.0 \pm 0.3$ nm), which will affect interfacial energy and modulus values. Moreover, Si_3N_4 is an opaque material and this would limit us to testing transparent samples.

Table 1 summarizes the Young's modulus of PDMS films obtained with two different lenses, i.e., PDMS and Si_3N_4. The same trend can be observed as before; i.e., the value of the Young's modulus increases with increasing sample treatment time. In addition, higher modulus values were obtained when using a PDMS lens. This may be due to two reasons. First, the PDMS film coated on the glass substrate consists of a thin layer of elastomer, with a thickness of ca. 800 nm, which is much smaller than the lens radius ($a = 1.15$ mm). There was a relatively high load applied on the lens (on the order of hundreds of micronewtons); therefore, the stress field extended over to the glass substrate in an uncontrolled way. The fact that we have not considered the modulus of the glass substrate could yield an apparent modulus value, which is higher than the true values. Moreover, the accuracy of using an equivalent modulus, averaged over the properties of both the indenter and the sample, has been recently questioned by Chaudhri et al.[38] On the other hand, the stiff Si_3N_4 lens indented into a much thicker PDMS layer and its elastic deformation can be neglected. The typical indentation depth by ATD is in this case around 0−3.3 μm (experimentally verified). The test with Si_3N_4 lens thus yields more accurate information about the PDMS film, and hence the obtained values are smaller and incidentally closer to the ones determined by macroscopic tests. We note again that the increased roughness of Si_3N_4 lens may also influence the obtained modulus values.

Analysis of the Length Scale Effects

Bulk mechanical properties are usually obtained by tensile and bending tests. The Young's moduli, measured as the initial slope of the stress−strain curves of untreated PDMS and 60 min treated PDMS, are essentially identical and consistent with the literature values.[39] (Typical stress−strain curves are shown in the Supporting Information.) Therefore, it can be concluded that the UV/ozone surface treatment does not affect the PDMS bulk mechanical properties. This is reasonable if one recalls that the UV/ozone treatment affects only a thin surface layer. However, it is worth to summarize the results achieved on different length scales in order to gain more insight into the effects of surface modification. To this end, Young's modulus measurements with different techniques, which gave information on mechanical performance at different depth scales, are summarized in Table 2.

The error bar stands for the standard deviation of the experimental data points. Two trends can be observed in Table 2. First of all, with two surface-sensitive mechanical techniques, AFM and ATD, the Young's modulus of UV/ozone-treated PDMS films increased with increasing treatment time (treatment dose). This could be explained by assuming that a silica-like layer is formed after surface treatment, which thickens with the dose and changes surface properties. Conversely, the bulk modulus was not significantly affected by the surface treatment. Second, the characteristic dimension of the probed length scale has an influence on the observed mechanical properties. With the same sample, comparing the AFM and ATD methods, the value of the elastic modulus decreased with increasing the length scale (from nano- to micrometer). The apparent surface moduli were also larger compared to the bulk values. It is worth to notice that differences in the Young's moduli for nano, meso, and macro length scales might also be related to the different time scales of the experiment, related to viscoelastic behavior. However, AFM nanoindentations were performed typically in 1 s, while the ATD measurements were carried out in 30 s. In both cases, the relaxation time of the PDMS samples can be considered much smaller than these time scales since the glass-to-rubber transition of PDMS is well below room temperature ($T_g = -123$ °C). Therefore, the different time scales alone cannot explain the different values of Young's moduli measured.

Early experimental observations have indicated that the length scale of observation has an influence on the mechanical properties observed for polymers as well as in metals[40] and ceramics.[41] For example, Lam and Chong have shown that a length-scale parameter associated with strain gradient yielding is influenced by the cross-link distance in epoxies.[42] Experiments on both thermosets and thermoplastics have shown that the hardness varies with different indentation depth.[43] It was concluded that this was due to a higher plastic yield stress in the presence of larger strain gradients. In our experiments, when the AFM tip penetrates into the PDMS surface, a highly three-dimensional strain field is formed. For untreated PDMS (see Figure 2a), the strain is approximately equal to $(l_{ACB} - l_{AB})/l_{AB}$. The strain can be estimated like $\Delta l/l_0 = (150 - 80)/80 = 0.875$, where $l_{AB} = 80$ nm and $l_{ACB} = 150$ nm for an indentation depth of 83 nm. For ATD measurements, the maximum contact radius is about 90 μm and the maximum indentation depth is about 3.3 μm; here $\Delta l/l_0 \approx 0.005$. Localization of the strains in a small region leads to the development of non-negligible strain gradients, and the magnitude of the gradient is dependent on the dimensions. In the work of Feichter et al.,[44] the influence of the initial crack tip radius on the strain distribution in the vicinity of the crack tip at the rubber surface was determined by an optical full field strain analysis method. They showed that while the crack tip was regularly blunted (half-circle shape) the strain gradient was low, and the crack tip was sharp with a higher strain gradient. The difference of the strain gradient may cause a length scale dependence of the modulus. In addition, adhesive forces play a significant role at the nanometer scale in indentation tests that would affect the real contact area during nanoindentation measurements. Furthermore, roughness of the indentor on a larger contact area will also affect the final results.

Conclusions

The length scale dependence of surface mechanical properties (surface Young's modulus) of UV/ozone-treated PDMS films was observed by probing the material with different techniques. AFM and ATD were used to measure the modulus from nano- to micrometer indentation depths, and the results were compared

Table 2. Young's Elastic Modulus Obtained across Different Length Scales[a]

	nanoindentation by AFM		microindentation by ATD with Si_3N_4 lens		
treatment time (min)	Young's modulus (MPa)	max indentation depth (nm)	Young's modulus (MPa)	max indentation depth (μm)	tensile test (MPa)
0	6.6 ± 0.4	86	3.1 ± 0.6	3.0	2.5 ± 0.2
15	24.7 ± 4.0	19	8.6 ± 0.8	2.8	
30	49.7 ± 4.7	13	9.0 ± 1.2	2.5	
60	$110. \pm 6.0$	9	13.1 ± 2.5	2.4	2.4 ± 0.3

[a] Si_3N_4 tip and lens were used as indentor.

with the bulk modulus. The elastic moduli varied with the size of the characteristic dimensions of the experiments. In addition, the values of surface elastic moduli increased with increasing treatment time. In general, indentation tests of surface mechanical properties are reasonably robust. However, the results must be interpreted with care and attention to the limitations of the analysis, and limitations of the instrument, keeping also in mind the type of material, and the length scale of the study.

Experimental Section

Tensile Test. The macroscopic mechanical properties of PDMS were evaluated with 5 mm × 5 mm × 100 mm polymer films. Tensile tests were carried out in duplicate at room temperature according to ASTM D882-91 specifications. A Zwick Z020 universal tensile tester equipped with a 500 N load cell was operated at a crosshead speed of 50 mm min^{-1}. The specimen deformation was derived from the grip-to-grip separation, which initially was 50 mm.

Nanoindentation by AFM. The nanoindentation tests were carried out using a NanoScope IV AFM (Veeco-Digital Instruments (DI), Santa Barbara, CA). A closed loop *Z*-axis PicoForce vertical engage scanner was used. Commercial silicon nitride tips (DI) were used as the indentors in the AFM indentation experiments. The cantilever specifications were as follows: length 350 μm, width 100 mm, thickness 13 mm, resonant frequency 50 kHz. The spring constants of the cantilevers ranged from 0.18 to 0.32 nN nm^{-1}, as obtained by the thermal tuning method of Hutter and Bechhoefer.[45] The radius of Si_3N_4 tip was verified by imaging suitable spherical gold colloid particles with a known diameter of 13 nm. From the measured width of the gold colloids, the effective radius of tip, R, can be calculated on the basis of geometrical considerations.[46]

AFM was operated in the force mode using a Z ramp rate of 1 Hz. Multiple force curves for each PDMS film were collected using the "point and shoot" mode of the AFM. Relative trigger thresholds were set to 20 nm. A series of automated indentations (up to 7 indents in 7 rows) were performed at different locations. Each individual force−distance curve was laterally separated by at least 1 μm from the preceding measurement to ensure that the observations are independent. All nanoindentation experiments were performed in an aqueous environment.

An indent was made by forcing the tip into the surface until the required cantilever deflection was reached. For each indent, a plot of the cantilever deflection vs displacement in the Z direction was recorded. These graphs were transformed into force (nanonewtons) vs tip penetration curves. The applied load F was determined as $F = k_c \Delta V/S$, where k_c is the spring constant, ΔV is the photodetector voltage change, and S is the cantilever sensitivity. The cantilever sensitivity was determined by taking force measurements using hard surfaces such as silicon. A MathCAD algorithm specifically developed for this purpose was used to extract Young's modulus from each data set.

Most AFMs plot forces vs a calculated Z position based on the anticipated response of the Z-piezo to a given voltage. However, undesirable piezo properties such as creep, hysteresis, and nonlinearity can make this position axis inaccurate, especially for irregular, noncyclic force plots. Thus, depth of penetration is difficult to determine due to piezo creep and hysteresis effects.[47] The PicoForce scanner (Veeco-Digital Instruments (DI), Santa Barbara, CA) incorporates a Z-axis capacitive sensor for closed loop positioning within 0.5 nm rms over 20 μm of travel toward and away from the sample stage. The closed-loop low-noise Z-axis sensor accomplishes the goal of obtaining the forces against an accurate position axis.

PDMS Film Preparation. All experiments were performed using an elastomeric PDMS kit manufactured by Dow Corning. Sylgard-184A (elastomer) and Sylgard-184B (curing agent) were used without modification and mixed at a mass ratio of 10:1. PDMS film preparation and UV/ozone treatment have been described in previous study.[6] Samples with different thickness values were used. PDMS films with thickness of 5 mm were applied in tensile tests. PDMS films with thicknesses of 200 μm and 800 nm were used in ATD measurements. Finally, PDMS films with thicknesses of 800 nm were utilized in AFM nanoindentation experiments.

Adhesion Testing Device (ATD). Contact mechanical measurements at a micrometer scale were carried out on a custom-built ATD setup (JKR apparatus) which was introduced in a previous study.[37] It was designed to measure the adhesion between two bodies, a hemisphere lens and a flat surface, where at least one of the bodies was elastic. In our experiments a PDMS film was attached directly to the upper glass microscope slide and mounted in the device as a stationary part. Si_3N_4 lens was purchased from HPSN, GIMEX (Technische Keramiek BV, Geldermalsen, The Netherlands). A PDMS lens or a Si_3N_4 lens was then firmly clamped into the holder frame and attached directly to the transducer head (Thames-side Maywood Ltd.) as a moving part. The contact area between lens and sample was continuously monitored by a CCD camera (Sony XC-999P) with a custom-made reflected light optical microscope utilizing a 10× magnification. The signals were transmitted to a National Instrument data acquisition board and connected to a desktop computer for subsequent data analysis and processing. Values of the temperature (T = 21 °C) and relative humidity (RH = 28%) were monitored by a combined sensor (T&RH) with an accuracy of ±3.5% (Sensiron SHT 11). The signals from the load cell, displacement transducer, T&RH sensor, and CCD camera were processed by a computer using a custom-written LabVIEW software. The use of the computer-controlled interface enabled a precise control of both the rate and displacement of the motor shaft.

Acknowledgment. Dr. Zheng Zhang is acknowledged for the tensile test. This work was financially supported by the Dutch Polymer Institute and by The Netherlands Foundation for Scientific Research (NWO).

Supporting Information Available: Representative stress and strain curves of untreated and 60 min treated PDMS and the detailed calculation of Young's modulus with continuum contact mechanics theory for AFM experiments by employing the hyperboloid tip shape model. This material is available free of charge via the Internet at http://pubs.acs.org.

References and Notes

(1) Syed Asif, S. A.; Colton, R. J.; Wahl, K. J. In *ACS Symposium Series*; Frommer, J., Overney, R., Eds.; Oxford University Press: Washington, DC, 2001; Vol. *781*, p 198.
(2) Jeong, K. H.; Liu, G. L.; Chronis, N.; Lee, L. P. *Opt. Express* **2004**, *12*, 2494–2500.
(3) Pelrine, R.; Kornbluh, R.; Pei, Q. B.; Joseph, J. *Science* **2000**, *287*, 836–839.
(4) McDonald, J. C.; Duffy, D. C.; Anderson, J. R.; Chiu, D. T.; Wu, H. K.; Schueller, O. J. A.; Whitesides, G. M. *Electrophoresis* **2000**, *21*, 27–40.

(5) Sia, S. K.; Whitesides, G. M. *Electrophoresis* **2003**, *24*, 3563–3576.
(6) Song, J.; Duval, J. F. L.; Stuart, M. A. C.; Hillborg, H.; Gunst, U.; Arlinghaus, H. F.; Vancso, G. J. *Langmuir* **2007**, *23*, 5430–5438.
(7) Vancso, G. J.; Hillborg, H.; Schönherr, H. *Adv. Polym. Sci.* **2005**, *182*, 55–129.
(8) Hillborg, H.; Gedde, U. W. *Polymer* **1998**, *39*, 1991–1998.
(9) Briscoe, B. J.; Sebastian, K. S. *Proc. R. Soc. London, Ser. A* **1996**, *452*, 439–457.
(10) Tranchida, D.; Kiflie, Z.; Piccarolo, S. *Macromolecules* **2007**, *40*, 7366–7371.
(11) Flores, A.; Calleja, F. J. B.; Attenburrow, G. E.; Bassett, D. C. *Polymer* **2000**, *41*, 5431–5435.
(12) Binnig, G.; Quate, C. F.; Gerber, C. *Phys. Rev. Lett.* **1986**, *56*, 930–933.
(13) Sarid, D. *Scanning Force Microscopy*; Oxford University Press: New York, 1991.
(14) Tsukruk, V. V.; Gorbunov, V. V.; Huang, Z.; Chizhik, S. A. *Polym. Int.* **2000**, *49*, 441–444.
(15) Tranchida, D.; Piccarolo, S. *Polymer* **2005**, *46*, 4032–4040.
(16) Domke, J.; Radmacher, M. *Langmuir* **1998**, *14*, 3320–3325.
(17) Vanlandingham, M. R.; Villarrubia, J. S.; Guthrie, W. F.; Meyers, G. F. *Macromol. Symp.* **2001**, *167*, 15–43.
(18) Vanlandingham, M. R.; McKnight, S. H.; Palmese, G. R.; Elings, J. R.; Huang, X.; Bogetti, T. A.; Eduljee, R. F.; Gillespie, J. W. *J. Adhes.* **1997**, *64*, 31–59.
(19) Briscoe, B. J.; Fiori, L.; Pelillo, E. *J. Phys. D* **1998**, *31*, 2395–2405.
(20) Reynaud, C.; Sommer, F.; Quet, C.; EI Bounia, N.; Duc, T. M. *Surf. Interface Anal.* **2000**, *30*, 185–189.
(21) Chizhik, S. A.; Huang, Z.; Gorbunov, V. V.; Myshkin, N. K.; Tsukruk, V. V. *Langmuir* **1998**, *14*, 2606–2609.
(22) Du, B. Y.; Tsui, O. K. C.; Zhang, Q. L.; He, T. B. *Langmuir* **2001**, *17*, 3286–3291.
(23) Raghavan, D.; Gu, X.; Nguyen, T.; Vanlandingham, M. R.; Karim, A. *Macromolecules* **2000**, *33*, 2573–2583.
(24) Du, B. Y.; Liu, J. P.; Zhang, Q. L.; He, T. B. *Polymer* **2001**, *42*, 5901–5907.
(25) Du, B. Y.; Zhang, J.; Zhang, Q. L.; Yang, D. C.; He, T. B.; Tsui, O. K. C. *Macromolecules* **2000**, *33*, 7521–7528.
(26) Drechsler, D.; Karbach, A.; Fuchs, H. *Appl. Phys. A: Mater. Sci. Process.* **1998**, *66*, S825−S829.
(27) Kajiyama, T.; Tanaka, K.; Satomi, N.; Takahara, A. *Macromolecules* **1998**, *31*, 5150–5151.
(28) Kaliappan, S. K.; Cappella, B. *Polymer* **2005**, *46*, 11416–11423.
(29) Tranchida, D.; Piccarolo, S.; Loos, J.; Alexeev, A. *Macromolecules* **2007**, *40*, 1259–1267.
(30) Sun, Y. J.; Akhremitchev, B.; Walker, G. C. *Langmuir* **2004**, *20*, 5837–5845.
(31) Hillborg, H.; Tomczak, N.; Olah, A.; Schönherr, H.; Vancso, G. J. *Langmuir* **2004**, *20*, 785–794.
(32) Johnson, K. L.; Kendall, K.; Roberts, A. D. *Proc. R. Soc. London, Ser. A* **1971**, *324*, 301–313.
(33) Sneddon, I. N. *Int. J. Eng. Sci* **1965**, *3*, 47–57.
(34) Swedlow, J. L. *Int. J. Fract. Mech* **1965**, *1*, 210–216.
(35) Olah, A.; Hillborg, H.; Vancso, G. J. *Appl. Surf. Sci.* **2005**, *239*, 410–423.
(36) Kayne, G. W. C.; Laby, T. H. *Tables of Physical and Chemical Constants*; Longman: Essex, 1985.
(37) Olah, A.; Vancso, G. J. *Eur. Polym. J.* **2005**, *41*, 2803–2823.
(38) Chaudhri, M. M. *J. Mater. Res.* **2001**, *16*, 336–339.
(39) Treloar, L. R. G. *The Physics of Rubber Elasticity*; Clarendon Press: Oxford, 1975.
(40) Fleck, N. A.; Muller, G. M.; Ashby, M. F.; Hutchinson, J. W. *Acta Metall. Mater.* **1994**, *42*, 475–487.
(41) Xu, Z. H.; Rowcliffe, D. *Surf. Coat. Technol.* **2002**, *161*, 44–51.
(42) Lam, D. C. C.; Chong, A. C. M. *J. Mater. Res.* **2001**, *16*, 558–563.
(43) Chong, A. C. M.; Lam, D. C. C. *J. Mater. Res.* **1999**, *14*, 4103–4110.
(44) Feichter, C.; Major, Z.; Lang, R. W. *Strain* **2006**, *42*, 299–304.
(45) Hutter, J. L.; Bechhoefer, J. *Rev. Sci. Instrum.* **1993**, *64*, 1868–1873.
(46) Engel, A.; Schoenenberger, C. A.; Muller, D. J. *Curr. Opin. Struct. Biol.* **1997**, *7*, 279–284.
(47) Hues, S. M.; Draper, C. F.; Lee, K. P.; Colton, R. J. *Rev. Sci. Instrum.* **1994**, *65*, 1561–1565.

MA800536Y